Numerical Study of Impulsive Motion Past a Rotating Cylinder for Newtonian and Non-newtonian Fluid

Sibasish Panda, Pratyush Kumar Mohanty, Prateek Gupta, and Chinu Routa

Abstract The flow phenomena for a rotating cylinder with the application of an impulsive translational motion is studied using ANSYS FLUENT 19R3. The study is carried out for power-law index $n = 1$ and 2 at a fixed Reynolds number (Re = 40) for different non-dimensional rotation rates ($\alpha = 0.5, 1, 2$). After the initial flow field reaches a steady state, the impulsive motion is applied by implementing a User defined function (UDF) which assigns a zero-inlet velocity. The time evolution of vorticity contours provides insights into the developing flow field after the impulsive motion. For both the power indices, it has been found that a higher rotational rate leads to faster flow stabilization and can be used for flow control. The flow phenomena is studied quantitatively in terms of aerodynamic coefficients. The Drag coefficient value decreases by 36.47% as value of α increases from 0.5 to 2 for $n = 1$. The sudden variation in force coefficients and their subsequent variation is used to interpret the effect of rotation rate on the disturbed flow field due to impulsive motion.

Keywords Rotating cylinder · Impulsive motion · Vortex shedding · Drag coefficient · Lift coefficient

1 Introduction

The study of fluid flow characteristics around a circular cylinder is a classical bluff body problem in fluid mechanics, with studies dating back to the fifteenth century. Flow over a cylinder can be classified as both an external and internal flow. Flow

S. Panda (✉) · P. K. Mohanty · P. Gupta · C. Routa
Department of Chemical Engineering, NIT Rourkela, Rourkela 769008, India
e-mail: S.Panda-2@student.tudelft.nl

S. Panda
Department of Mechanical, Materials, and Maritime Engineering, Technische Universiteit Delft, Delft, Netherlands

P. Gupta
Davidson School of Chemical Engineering, Purdue University, Lafayette, USA

K. M. Singh et al. (eds.), *Fluid Mechanics and Fluid Power, Volume 2*, Lecture Notes in Mechanical Engineering, https://doi.org/10.1007/978-981-99-5752-1_53

over a cylinder in an unconfined domain can be categorized as an external flow, whereas flow over a cylinder in a confined domain can be categorized as an internal flow. Despite having a simple geometry, flow past a circular cylinder is a baseline example of more complicated flows having significant real-life applications. These applications often involve fluids flowing over complex geometries, like missiles, bridge pillars, jets, wings, submarines, and turbines. Moreover, research pertaining to flow around cylinders serves as a foundation for understanding various industrially significant applications such as heat exchangers, cooling towers, nuclear reactors, chimney stacks, and other offshore structures. Over the years, several studies have employed a wide range of Reynolds numbers to investigate laminar to turbulent transition in the wake, boundary layer transition, unsteady vortex shedding, and turbulent separation. As a fundamental method for flow control, rotating cylinders have gained significant traction over stationary cylinders. Cylinder motion can be classified into two types–forced (externally applied force) or free motion (movement due to fluid flow forces). An impulsive motion, which can be categorized as a forced motion, significantly enhances flow control by altering the flow field drastically. This work aims to develop an understanding and compare fluid flow characteristics over an impulsively rotating circular cylinder for Newtonian and for non-Newtonian fluid using the Carreau Model.

2 Literature Review and Objective

In recent decades of fluid dynamics research, the study of flow phenomena around static and rotating circular cylinders has attracted many researchers. Similarly, studies of impulsive cylinder motion have gained attention due to its application in many real-life scenarios. However, there has been no work on flow past impulsively moving rotating cylinder to the best knowledge of authors. This section aims to provide a brief overview of relevant past studies and their significant findings. Streeter [1], in his book, described several experimental and numerical investigations of the flow dynamics that have been described using hydrodynamic parameters such as drag and lift coefficients, vortex shedding, wake generation. One of the first comprehensive review studies of flow past a steady circular cylinder highlighted vital flow kinematics such as the range of Reynolds number for flow separation, the increase of wake Length, and flow transition with Reynolds number [2, 3]. Chew et al. [4] numerically investigated the shedding of vortices and the formation of wakes in a two-dimensional viscous incompressible flow generated by an impulsively rotating circular cylinder by a hybrid vortex scheme. The results indicated a critical value of $\alpha = 2$ when a closed streamline began to circulate around the cylinder. Prasad et al. [5] investigated the effect of rotation on flow across a cylinder for different blockage ratios ($\beta = 0$–50%), non-dimensional rotational velocity ($\alpha = 0$–2), and Reynolds number (Re = 35–170). They concluded that under counter clockwise rotation, a downward lift force was generated, which increased with increasing blockage ratio. Panda et al. [6] explored power-law fluid flow over a rotating cylinder for $0.1 \leq \text{Re} \leq 40$ and

non-dimensional rotational velocity $0 \leq \alpha \leq 6$. They found that at low Reynolds numbers, the power-law index has a much stronger influence on drag and lift than at high Reynolds numbers. Thakur et al. [7] explored the steady two-dimensional flow of incompressible Bingham plastic fluids past a rotating circular cylinder for $0.1 \leq \mathrm{Re} \leq 40$ and non-dimensional rotational velocity $0 \leq \alpha \leq 5$. They found an increase in the Bingham number with a decrease in the rotational velocity.

Hourigan et al. [8] studied the vortex dynamics of the flow past a suddenly arrested translating circular cylinder. They found that the Kármán wake vortices roll up on each side of the cylinder to form two larger structures over a long distance. Ta Phuoc Loc [9] numerically investigated the mechanism of creating secondary vortices behind an impulsively started circular cylinder with greater precision numerical technique at $\mathrm{Re} = 300$, 550 and 1000. He studied the properties of the creation and the development of the primary and secondary vortices and verified it with the available experimental data. Koumoutsakos et al. [10] investigated the impulsively started Newtonian flow around a circular cylinder via high-fidelity computations. They showed that the interaction of primary and secondary vorticity is the underlying mechanism for drag reduction and increase. Collins et al. [11] studied the initial flow in a viscous fluid in the direction normal to an infinite circular cylinder that is started impulsively from rest with uniform velocity. They found that the friction and pressure drag are equal for all Reynold numbers at the start of the motion. Pantokratoras [12] has numerically investigated the flow of Carreau fluid over a cylinder using drag and lift coefficient and reported the increase in drag coefficient for shear-thickening fluids and a decrease for shear-thinning fluid on increasing the Carreau number (Cu). Ohta et al. [13] studied numerical simulations of Carreau model fluid flows past a circular cylinder. They found the effective Reynolds number advocated in this study allows one to fully describe the flow state of Carreau model fluids past a circular cylinder on par with Newtonian fluid flows.

Based on the literature survey on the flow around a circular cylinder, it is observed that a majority of the work describes the effects of rotation and impulsive motion separately. Furthermore, little is known about the impulsive motion and rotation effects on aerodynamic parameters like drag and lift coefficients. The present work aims to study and compare the flow phenomenon on an impulsively moving rotating circular cylinder for different power-law indices and explain the behaviour of the aerodynamic parameters. As the shear-thickening fluid for power-law index $n = 2$ was modelled, the Carreau model was chosen over the power-law model.

3 Mathematical Modelling

3.1 Governing Equations

The flow is assumed to be 2-D incompressible with a uniform inlet velocity before the impulse. The continuity and momentum equation for the flow can be written as

Continuity equation

$$\frac{\partial u_x}{\partial x} + \frac{\partial u_y}{\partial y} = 0. \tag{1}$$

Momentum equation

$$\rho\left(\frac{\partial u_x}{\partial t} + \frac{\partial (u_x u_x)}{\partial x} + \frac{\partial \left(u_x u_y\right)}{\partial y}\right) = -\frac{\partial p}{\partial x} + \left(\frac{\partial \tau_{xx}}{\partial x} + \frac{\partial \tau_{yx}}{\partial y}\right) \tag{2}$$

$$\rho\left(\frac{\partial u_y}{\partial t} + \frac{\partial \left(u_x u_y\right)}{\partial x} + \frac{\partial \left(u_y u_y\right)}{\partial y}\right) = -\frac{\partial p}{\partial y} + \left(\frac{\partial \tau_{xy}}{\partial x} + \frac{\partial \tau_{yy}}{\partial y}\right) \tag{3}$$

Equation of Carreau model

$$\mu = \mu_1 + (\mu_0 - \mu_1)[1 + (\lambda\gamma)^2]^{\frac{n-1}{2}} \tag{4}$$

3.2 Boundary Conditions

At the domain boundaries and cylinder wall, the boundary conditions for the present problem are written as follows:

- At the inlet, before the introduction of impulse, a constant uniform flow profile in the x-direction and zero velocity in the y-direction can be written mathematically as

$$u_x = u_\infty \text{ and } u_y = 0 \tag{5}$$

After the introduction of impulse, zero velocity is assigned to both x and y velocity components

$$u_x = 0 \text{ and } u_y = 0 \tag{6}$$

- On cylinder surface: No-Slip boundary condition is applied throughout. It can be written as

$$u_x = u_y = 0 \tag{7}$$

- At upper and lower wall: Symmetry boundary condition in the x direction is applied. It can be written as

$$\frac{\partial u_x}{\partial y} = 0 \text{ and } u_y = 0 \tag{8}$$

- At the outlet: The outflow boundary condition is used throughout. The outflow condition corresponds to zero diffusion fluxes in the direction normal to the outlet planes. It is used for all the dependent variables.

$$\frac{\partial u_x}{\partial x} = 0; \frac{\partial u_y}{\partial x} = 0 \tag{9}$$

3.3 Numerical Methodology

Finite-volume method (FVM)-based commercial software ANSYS FLUENT 19R3 is used to for the current study. Figure 1 shows the computational domain used for the study. Full pressure–velocity coupling is achieved using a pressure-based coupled solver, resulting in faster convergence. The convective term in the flow equation is discretized using Linear Upwind Differencing (LUD) which uses a three-point stencil to give second-order accuracy, whereas the approximation for the diffusion term is automatically second-order accurate. Discretization with respect to time is first-order implicit, magnifying the stability envelope several-fold. A convergence criterion of 10^{-6} is set for the residuals of velocity and continuity terms. The accuracy of our results has been ensured by performing the grid, domain, and time independence tests.

A zoomed-in view of multi-block structured mesh as shown in Fig. 2 is used due to the accuracy and stability of solution provided by the structured mesh over the unstructured mesh.

3.4 Grid Independence Test

A square domain of varying dimensions is considered for the grid independence test**.** The independence test is performed at Reynolds number Re = 40 and dimensionless rotational speed $\alpha = 0.5$ for a Newtonian fluid. Based on the increasing accuracy of aerodynamic parameters shown in Table 1, an optimum grid G2 is finalized for the current study.

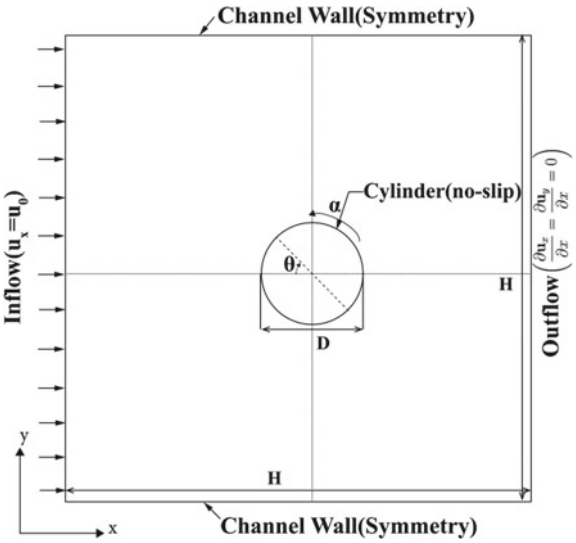

Fig. 1 Schematic of the computational domain for initial conditions

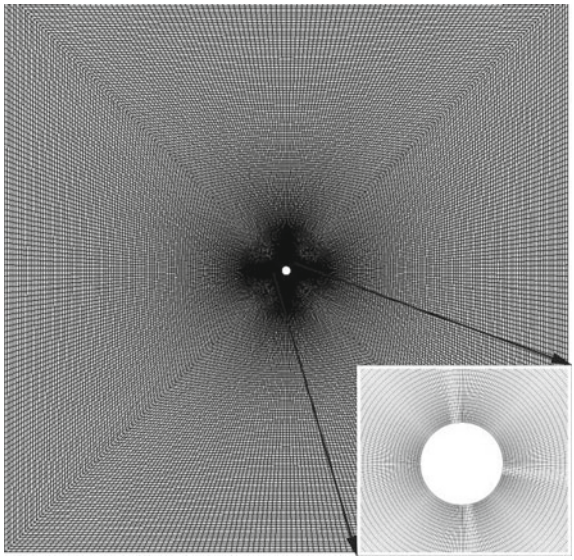

Fig. 2 Multi-block structured mesh used for the study

Table 1 Grid independence test

Grid (no. of nodes)	Drag coefficient (C_D)	Lift coefficient (C_L)
G1 (18,800)	0.906	−5.60
G2 (55,200)	0.889	−5.629
G3 (109,200)	0.865	−5.635

Table 2 Comparison of present results with literature

Re	α	n	Present values		Literature values	
			C_D	L_W	C_D	L_W
40	2	1	0.84	–	0.83 [6]	–
40	0	1	1.53	2.24	1.50 [12]	2.15
40	0	2	4.52	0.27	4.33 [12]	0.29

4 Results and Discussion

4.1 Validation

Relevant validatory studies have been performed to establish the suitability of chosen numerical methodology. Validation cases Pantokratoras [12] have been used to verify the suitably chosen methodology for fluid flow over stationary cylinder, whereas cases from Panda and Chhabra [6] have been used to validate the same methodology for rotational effects. Table 2 is presented to compare the obtained force coefficient values with literature values. The obtained result shows excellent agreement with the result presented in the literature with a maximum of 4.38% deviation.

4.2 Vortex Shedding Characteristics

Vorticity contours for both the power-law indices have been presented in Fig. 3 to give a qualitative understanding of the flow phenomena. Positive (Counter-Clockwise) vortices are shown by solid lines and Negative (Clockwise) vortices are shown by dashed lines in the vorticity contours. The flow fields are contrasted at different values of α to understand its significance. In this study we have denoted the developed flow field with t = 0, at which the flow fully develops with the initial inlet condition. Subsequently, we demonstrate the development of flow field at different instances of time after the impulse.

4.2.1 Power-Law Index $n = 1$

We notice the primary (P) vortices surrounding the cylinder at all values of α. These primary vortices are formed due to boundary layer separation and the formation of a recirculation zone behind the cylinder. As expected, at $\alpha = 2$, the cylinder tries to wrap the nearby vorticity around itself due to extremely high rotational inertia. We observe this dynamic steady state pattern up until $t = 2.5$. At $t = 2.5$, with the implementation of the User Defined Function (UDF) the flow velocity drops to zero instantaneously. In fact, this sudden drop in velocity can be characterized as

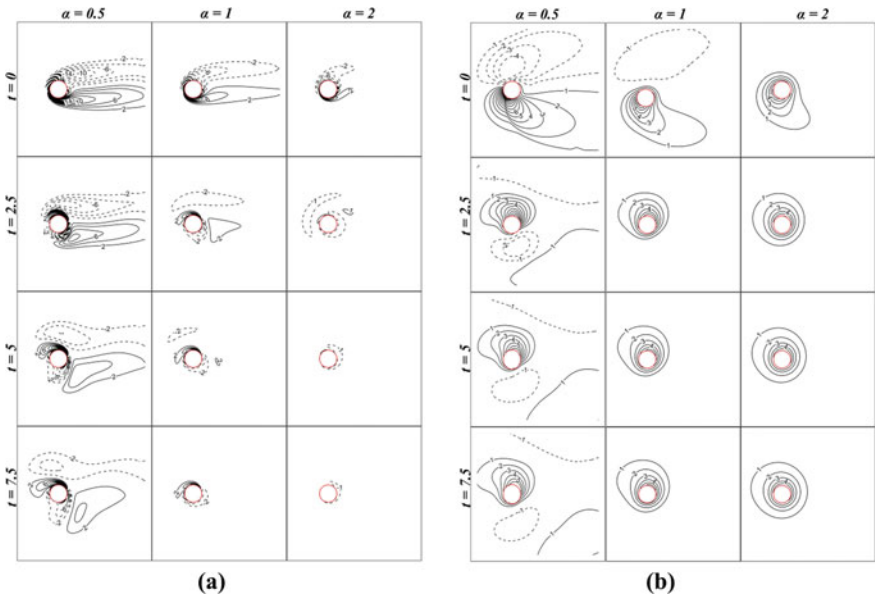

Fig. 3 Comparison of time evolution of vorticity for different rotational rates for **a** $n = 1$ **b** $n = 2$

impulsive. We notice that the primary (P) vortices have detached from the cylinder surface, and the void is filled in by the secondary (S) vortices. Due to the cylinder's continued rotation, these secondary vortices also start to wrap around the surface. As we move from $\alpha = 0.5$ to $\alpha = 2$, the amount of negative vorticity engulfing the cylinder increases. Moreover, as α increases, the diffusion of the primary vortices accelerates. As we move to the subsequent time-instants ($t = 5$ and $t = 7.5$), we notice that for $\alpha = 0.5$, the negative/clockwise secondary vortex starts to spill. Whereas it remains highly compact for $\alpha = 2$. Again, this can be attributed to the increased rotational inertia of the flow. Furthermore, at $t = 5$ and 7.5, the cylinder space is completely devoid of any hint of primary vortex for $\alpha = 2$. In addition, the cylinder is only surrounded by negative vorticity at $\alpha = 2$ for the time instant $t = 7.5$. Thus, it can be summarized that higher α values can lead to accelerated diffusion of the vortices.

4.2.2 Power-Law Index $n = 2$

Similar to the Newtonian case, we observe primary vortices surrounding the cylinder at $t = 0$. However, one striking feature to note is the magnitude of the vorticity contours and the extent to which they are spread out. Higher inertia of the shear-thickening fluid leads to the development of enveloping vortex for $\alpha = 2$ even before the application of impulse. Implementation of UDF at $t = 2.5$ leads to detachment of primary vortices (P) and development of secondary vortices (S) for $\alpha = 0.5$ whereas

for $\alpha = 1$ and $\alpha = 2$ no visible detachment is observed. The existing counter clockwise (CCW) vortices however change their orientation. The vortices take longer time to decay in comparison to their Newtonian counterparts for all the rotational rates. This behaviour of the flow field can be attributed to shear-thickening nature of the working fluid.

4.3 Variation of Force Coefficients with Time and Rotation Speed

In this section, the variation of force coefficients, for both power-law indices, through the impulsive motion is discussed with the help of Fig. 4. Both the drag and lift coefficients are studied once the flow with the initial inlet condition is fully developed, i.e., at $t = 0$. The sudden spike observed for both drag and lift coefficients can be attributed to the impulsive motion introduced at $t = 2.5$. The dip for drag coefficient can be attributed to a change in flow inertia with the introduction of impulse that leads to an instant detachment of the Primary vortices (P) and subsequent development of Secondary vortices (S). For $n = 1$, the magnitude of dip in drag coefficient is less in comparison to the dip for $n = 2$. The spike in lift coefficient for the Newtonian fluid, can be attributed to detachment and subsequent development of oppositely signed vortices over time. However, for the non-Newtonian case there is no spike for $\alpha = 1$ and $\alpha = 2$ due to non-detachment of vortices. This observation can be attributed to increased inertial properties of the shear-thickening fluid. The variation in coefficients has been studied till they reach a steady state after the introduction of the impulse. An important observation is concluded from observation of time taken, through variation of force coefficients, for the flow to reach steady state after the impulsive motion. For $n = 1$, the time taken by $\alpha = 2$ is less that the amount of time taken by $\alpha = 0.5$. This can be attributed to a faster dissipation rate at $\alpha = 2$ leading to faster stabilization of flow.

5 Conclusions

In this paper application of impulsive translational motion on a rotating cylinder at different rotation rates ($\alpha = 0.5, 1, 2$) for a Newtonian fluid and shear-thickening fluid having power-law index $n = 2$ is studied. The Reynolds number based on cylinder diameter is kept constant. The non-dimensional rotation rate is varied so as to study the effect of rotation on disturbed flow field due to impulsive motion. In order to interpret the results both qualitatively and quantitatively, vorticity contours and force coefficients have been studied respectively. A comparison of the time evolution of vorticity contours for different rotational rates shows the enhanced dissipation rate at a higher rotational rate. In a quantitative sense, the sudden change in sign of

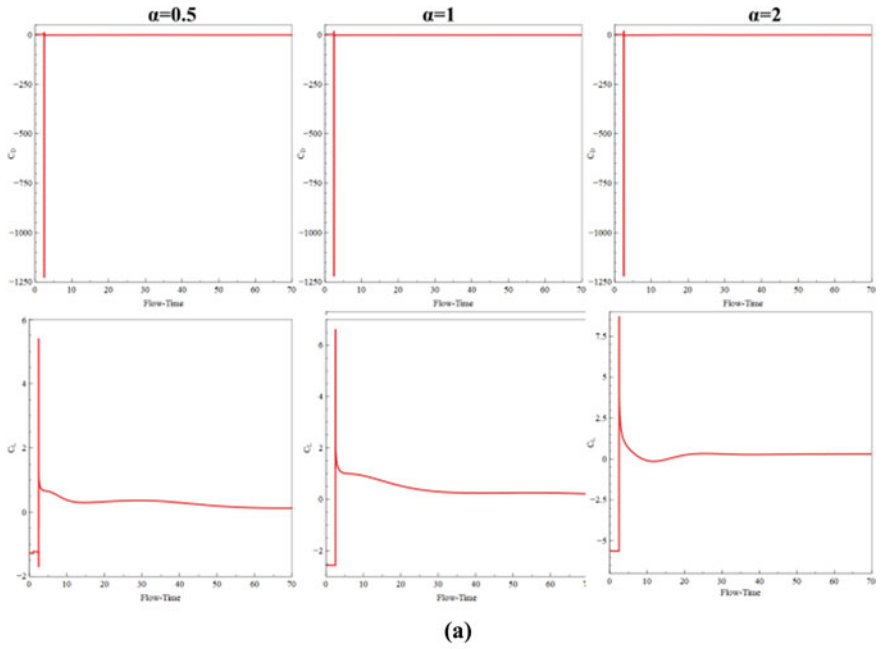

Fig. 4 Variation of force coefficients through the impulsive motion for **a** $n = 1$ **b** $n = 2$

force coefficients explain the formation of oppositely signed vorticity contours with the application of impulsive motion for the Newtonian fluid and the change in the orientation of enveloping vortices for higher rotational rate for non-Newtonian fluid. Moreover, a significant amount of time is taken, which is monitored here by variation of force coefficients, for $\alpha = 0.5$ in comparison to $\alpha = 2$ establishes the fact that a higher rotation rate leads to better flow control. This study can be further extended to investigate the effect of multiple impulses and their effect on higher rotational rates.

Abbreviations

Nomenclature

C_{D}	Drag Coefficient
C_{L}	Lift Coefficient
D	Diameter of Cylinder (m)
H	Height of the computational domain (m)
L_{W}	Wake length (m)
u_∞	Free stream velocity (m/s)
u_x	x-Component of velocity (m/s)
u_y	y-Component of velocity (m/s)
p	Pressure (Pa)
τ_{ij}	Extra stress tensor (Pa)
n	Power-law index
μ_0	Zero shear viscosity (Pa s)
μ_1	Infinity-shear viscosity (Pa s)

Greek Symbols

α	Non-dimensional rotational velocity [$= D\,\omega/2\,u_\infty$]
ρ	Density of working fluid
ω	Angular velocity

References

1. Streeter VL (1961) Handbook of fluid dynamics. McGraw-Hill, New York
2. Zdravkovich MM (1997) Flow around circular cylinders, 1 fundamentals. Oxford University Press, New York

3. Zdravkovich MM (2003) Flow around circular cylinders, 2 applications. Oxford University Press, New York
4. Chew YT, Cheng M, Luo SC (1995) A numerical study of flow past a rotating circular cylinder using a hybrid vortex scheme. J Fluid Mech 299:35–71
5. Prasad K, Paramane SB, Agrawal A, Sharma A (2011) Effect of channel-confinement and rotation on the two-dimensional laminar flow and heat transfer across a cylinder. Num Heat Trans Part A Appl 60(8):699–726
6. Panda SK, Chhabra RP (2010) Laminar flow of power-law fluids past a rotating cylinder. J Nonnewton Fluid Mech 165(21–22):1442–1461
7. Thakur P, Mittal S, Tiwari N, Chhabra RP (2016) The motion of a rotating circular cylinder in a stream of Bingham plastic fluid. J Nonnewton Fluid Mech 235:29–46
8. Sheard GJ, Leweke T, Thompson MC, Hourigan K (2007) Flow around an impulsively arrested circular cylinder. Phys Fluids 19(8):083601
9. Loc TP (1980) Numerical analysis of unsteady secondary vortices generated by an impulsively started circular cylinder. J Fluid Mech 100(1):111–128
10. Koumoutsakos P, Leonard A (1995) High-resolution simulations of the flow around an impulsively started cylinder using vortex methods. J Fluid Mech 296:1–38
11. Collins WM, Dennis SCR (1973) The initial flow past an impulsively started circular cylinder. Quart J Mech Appl Math 26(1):53–75
12. Pantokratoras A (2016) Steady flow of a non-Newtonian Carreau fluid across an unconfined circular cylinder. Meccanica 51(4):1007–1016
13. Ohta M, Toyooka T, Matsukuma Y (2020) Numerical simulations of Carreau-model fluid flows past a circular cylinder. Asia-Pac J Chem Eng 15(6):e2527